SP Science Press

ARTICLE

Effect of Micro/nano-SiC$_P$ on Microstructure and Properties of Electroless Ni-P-SiC$_P$ Composite Coatings

Chao Shuang[1], Cao Jingjing[1,2], Li Hezong[1,2], Fan Lei[3], Yang Junheng[1], Harvey Christopher Martin[4]

[1] School of Mechanical and Equipment Engineering, Hebei University of Engineering, Handan 056038, China; [2] Key Laboratory of Intelligent Industrial Equipment Technology of Hebei Province, Handan 056038, China; [3] School of Mechanical and Electrical Engineering, China University of Mining and Technology (Beijing), Beijing 100083, China; [4] Department of Aeronautical and Automotive Engineering, Loughborough University, Loughborough LE11 3TU, UK

Abstract: Ni-P-SiC$_P$ coatings were deposited on 42CrMo steel by electroless plating. The surface morphologies and phase structures of the Ni-P-SiC$_P$ coatings processed under different SiC$_P$ concentrations at different heat treatment temperatures were analyzed. The microhardness, corrosion resistance, and wear resistance of the Ni-P-SiC$_P$ coatings were studied. Results show that Ni-P-SiC$_P$ coatings exhibit cauliflower-like morphology. Increasing the SiC$_P$ concentration can reduce the size of cellular structure. The microhardness and corrosion resistance are initially increased and then decreased with the increase in SiC$_P$ concentration. The maximum microhardness and corrosion potential are 7379 MPa and −0.363 V, respectively, when the SiC$_P$ concentration is 5 g/L. The Ni-P-SiC$_P$ coatings exhibit an amorphous structure, and the width of the diffuse diffraction peak becomes narrower with the increase in SiC$_P$ concentration. It is suggested that SiC$_P$ inhibits the deposition of P and promotes the microcrystalline transformation. After heat treatment at 350 °C, the Ni-P-SiC$_P$ coatings are crystallized, resulting in the precipitation of Ni$_3$P phase. Heat treatment at 400 °C for 1 h maximizes the structure. The synergistic effect of the Ni$_3$P precipitate phase and SiC$_P$ dispersion phase promotes the densification of the cellular structure, leading to the optimal microhardness (13 828 MPa), optimal corrosion resistance (−0.277 V), and excellent wear resistance. The wear mechanism is dominated by micro-cutting abrasive wear with slight adhesive and oxidative wear.

Key words: 42CrMo steel; Ni-P-SiC$_P$ composite coatings; heat treatment; corrosion resistance; wear mechanism

42CrMo steel, classified as P110 grade petroleum steel, has excellent strength and toughness after quenching and tempering. The material is commonly employed in oil-well pipes for oil and gas mining machinery. With the increase in the depth of drilling of petroleum reservoirs, oil-well pipes need to withstand elevated temperature and pressure, wear from rock layers, and erosion from corrosive media, such as H$_2$S and H$_2$[1]. These harsh conditions significantly impact the performance and service life of oil-well pipes. To sufficiently utilize the favorable mechanical properties of 42CrMo steel and to improve its wear and corrosion resistance, surface protection technique emerges as the primary solution. Electroless plating, as a surface treatment method, deposits metal onto the substrate surface, forming a film layer through a spontaneous chemical reaction at low temperatures. This technique imparts excellent wear resistance, corrosion resistance, and other characteristics, such as good optical, electrical, and magnetic properties to the substrate[2]. In comparison to other surface techniques, such as thermal diffusion, laser beam, electron beam, and vapor deposition, electroless plating operates at a low deposition reaction temperature (60–90 °C), minimally impacting substrate performance. Moreover, the equipment and process are simple, efficient, and cost-effective, being widely applicable across various industrial sectors. Currently, electroless plating technique has evolved from binary plating to ternary and multi-component plating, even advancing to composite plating. Electroless composite plating incorporates the second-

phase hard particles or flexible particles onto the original binary plating, facilitating the co-deposition of particles and metal ions on the substrate surface. This approach further enhances the wear resistance or friction reduction capability of the coatings[3].

In the selection of second-phase particles for electroless composite plating, diamond, SiC, Al_2O_3, WC, and B_4C are selected to enhance hardness and wear resistance[4–8], and particles are chosen to improve the self-lubricity of the coatings, including CaF_2, $(CF)_n$, polytetrafluoroethylene (PTFE), and MoS_2[9–11]. SiC is a covalent material (88% covalent state and 12% ionic state). As a hard ceramic particle, SiC has superior wear resistance, corrosion resistance, heat resistance, high strength, and low cost, compared with other hard particles[12–15], and it is frequently employed as a ceramic second-phase reinforced particle in metal substrate composites or high-entropy alloy coatings[16–21]. Adding SiC particles into the electroless plating solution for co-deposition with Ni and P can improve the performance of electroless plating. Chintada et al[22] investigated the effect of various surfactants on electroless Ni-P-SiC coatings and reported that the cationic surfactants contribute to the uniform dispersion of SiC nanoparticles in the plating solution. The Ni-P-SiC coating prepared with SiC concentration of 2 g/L has optimal wear and corrosion resistance after heat treatment at 400 ° C. Masallb et al[23] explored the erosion-corrosion wear performance of Ni-P-SiC composite coatings in heavy crude oil fuel. Compared with the base AISI 316 stainless steel, the Ni-P-SiC composite coatings exhibit outstanding erosion-corrosive wear resistance after heat treatment at 600 °C. Liu et al[24] fabricated Ni-P-SiC composite coatings on the surface of 70vol% SiC/Al composite material to enhance the solderability. The effect of different SiC contents and heat treatment temperatures on the thermal expansion coefficient between the Ni-P-SiC composite coatings and SiC/Al matrix was researched. Results indicated that the thermal expansion coefficient was initially decreased and then increased with the increase in SiC content from 0 g/L to 9 g/L, and the optimal thermal expansion coefficient was achieved at 6 g/L SiC. The maximum interface bonding strength between the Ni-P-SiC coatings and the SiC/Al substrate reached 84.9 N when the preparation condition was 3 g/L SiC with heat treatment at 200 °C. Gao et al[25] prepared a Ni-P/SiC/PTFE modified layer on 316L stainless steel surface by two-step method: electrodepositing Ni-P/SiC and impregnating PTFE. The study focused on the corrosion resistance, revealing that the composite coatings had a uniform and dense multi-layer structure with thickness of 23.2 μm, exhibiting excellent corrosion resistance (self-corrosion current density, 0.09 μA/cm²) in strong acid and high-temperature environments after heat treatment at 350 ° C. Farzaneh et al[26] studied the influence of heat treatment temperature on the corrosion resistance of Ni-P-SiC nanocomposite coatings. The Ni-P-SiC coatings exhibited a uniform and dense structure after heat treatment at 400 ° C, displaying relatively lower corrosion current density and higher polarization resistance.

Ahmadkhaniha et al[27] used electroplating technique to fabricate Ni-P coatings on low alloy steel with SiC particles (100 nm). Ball-on-disk wear tests showed that the Ni-P-SiC composite coatings had higher hardness and better wear resistance after heat treatment at 400 ° C. Ghavidel et al[28] prepared the Ni-P/nano-SiC composite coatings by electroless plating on the surface of AZ31 magnesium alloy. By adding nano-SiC particles, the corrosion resistance and wear resistance of the coatings can be improved. At the same time, the nanoparticles are easy to aggregate. The composite coating has better corrosion resistance and wear resistance with the addition of 1 g/L nanoparticles. Khodaei et al[29] deposited Ni-P coatings with nano-SiC particles on carbon steel by electroless plating. The hardness of the composite coatings after heat treatment increased by about 25% and the wear amount reduced by nearly 48%. The composite coatings prepared with 1 g/L SiC particles have better corrosion resistance and wear resistance.

Research results show that the Ni-P-SiC composite coatings have better corrosion resistance and wear resistance before and after heat treatment. It is reported that the addition of nano-SiC particles can fill the micropores on the surface of Ni-P coating, thereby improving the compactness and the corrosion resistance of the composite coatings. In addition, the increase in hard particles can resist external physical stimulation, thereby increasing wear resistance. However, the researches of Ni-P-SiC composite coatings mainly focus on the effect of nanoparticles on the coating performance. The agglomeration of nano-SiC particles requires auxiliary high-energy dispersion technique during the deposition process. Although the high-energy dispersion solves the problem of nano-SiC particle agglomeration, it also leads to the decrease in the stability of plating solution. To avoid the agglomeration of nano-SiC particles, the addition amount should not be too large (the reported appropriate amount is about 1 g/L). Thus, the enhancement in the wear resistance and corrosion resistance of the coatings is restricted. Compared with nano-SiC particles, micro/nano-SiC particles (SiC_p) have a smaller specific surface area and less severe agglomeration phenomenon. They can effectively reduce the cost of dispersion processing of nano-SiC particles and avoid the impact of dispersion processing on the stability of plating solution. It can also increase the SiC particle content and improve the corrosion and wear resistance of the coating. Currently, the effect of the addition of SiC_p as reinforcing phase into the Ni-P plating solution is rarely investigated.

Therefore, in this research, the effects of SiC_p concentration on the morphology, composition, phase structure, micro-hardness, and corrosion resistance of electroless Ni-P-SiC_p composite coatings were investigated using 42CrMo oil-well tube steel as substrate. The heat treatment process and wear resistance were studied to reveal the wear mechanism of Ni-P-SiC_p composite coatings. This research provides a theoretical basis for the extensive application of Ni-P-SiC_p composite coatings in the oil-well tube and other wear and corrosion conditions.

1 Experiment

The quenched and tempered 42CrMo steel after rolling was used as the matrix, and specimens of 20 mm×12 mm×7 mm were fabricated through electro-discharge cutting. To facilitate the balanced suspension, a thin slit of approximately 5 mm in length was beveled along the side. Prior to further treatment, the specimen surface was meticulously processed for smoothness and flatness. Sequential polishing was conducted using 180#, 400#, 800#, 1000#, and 1500# sandpaper followed by ultrasonic cleaning. After these preparations, the specimens were pre-treated using the alkaline degreasing solution and pickling activation solution. The formulation of the alkaline degreasing solution is shown in Table 1. The solution of 37wt% HCl was used for pickling. It is imperative to conduct thorough ultrasonic cleaning after each treatment step to eliminate residual treatment solution and reactants from the preceding treated surfaces.

The SiC_P second phase with 0.5 μm in size was chosen for tests and introduced into the electroless plating solution. To modify the surface tension of SiC_P solution and to ensure the uniform dispersion of particles, an infiltration treatment was conducted[30]. The infiltration solution consisted of 37% hydrochloric acid and deionized water with the volume ratio of 1:25. Approximately 50 g SiC_P second phase was treated with 250 mL infiltration solution. Thorough infiltration of SiC_P was achieved by magnetic and ultrasonic stirring. After adequate infiltration, the SiC_P second phases were repeatedly cleaned with deionized water until the upper layer of the SiC suspension became transparent. Subsequently, the SiC_P second phases were fully dried using drying box and then sealed. Fig. 1 illustrates the morphologies of SiC_P second phases before and after the infiltration treatment. Before infiltration treatment, SiC_P exhibited obvious agglomeration phenomenon. The soft agglomeration of SiC_P second phases could be effectively eliminated after infiltration, promoting the uniform dispersion in the plating solution during subsequent plating processes.

During the electroless plating process, Ni and P were preferentially deposited at the optimal active sites on the substrate surface. To ensure the co-deposition of SiC_P second phases with Ni and P on the uniformly active surface, the pre-treated substrate was pre-plated with Ni-P processing. To maintain the consistency in coating performance and to minimize the influence of plating solution composition, the pre-plating solution and the electroless plating solution shared the same formulation, as listed in Table 2. The Ni-P pre-plating process was conducted for 30 min, and the resultant

Table 1　Formulation of alkaline degreasing solution

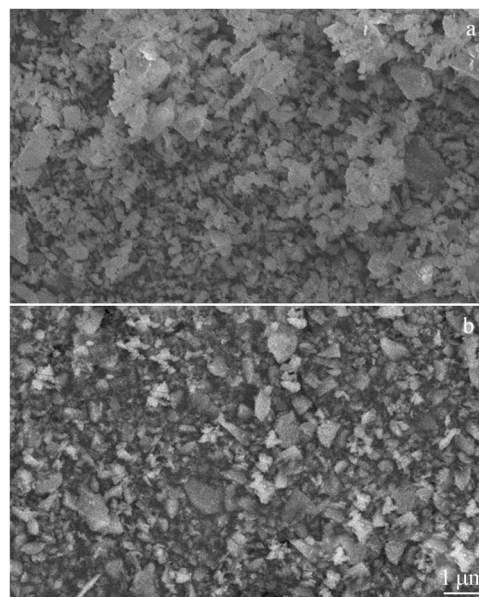| Component	Molecular formula	Content/ g·L^{-1}
Sodium carbonate	Na_2CO_3	30
Sodium hydroxide	NaOH	28
Trisodium phosphate dodecahydrate	$Na_3PO_4\cdot12H_2O$	10

Fig.1　Morphologies of SiC_P second phases before (a) and after (b) infiltration

Table 2　Components in electroless plating solution

Component	Molecular formula	Content/g·L^{-1}
Nickel sulfate	$NiSO_4\cdot6H_2O$	24
Sodium hypophosphite	$NaH_2PO_2\cdot H_2O$	30
Sodium citrate	$C_6H_5NaO_2\cdot3H_2O$	20
Ammonium acetate	CH_3COONH_4	10
Succinic acid	$C_4H_6O_4$	12
Glycine	$C_2H_5NO_2$	8
Silicon carbide	SiC_P	0, 1, 3, 5, 7, 9

surface morphology is shown in Fig. 2. The surface morphology of the Ni-P pre-plating surface is characterized by uniform and flat cells, offering a consistent active surface for subsequent composite plating. For the Ni-P-SiC_P composite coating, the plating time was 30 min, and SiC_P concentrations were 0, 1, 3, 5, 7, and 9 g/L. The entire preparation process for the electroless plating of Ni-P-SiC_P composite coating is outlined in Fig. 3, and Fig. 4 illustrates the schematic diagram of the experiment device for electroless plating.

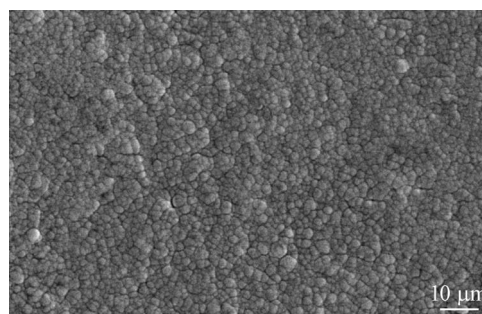The Ni-P-SiC_P composite coatings were heat-treated in a

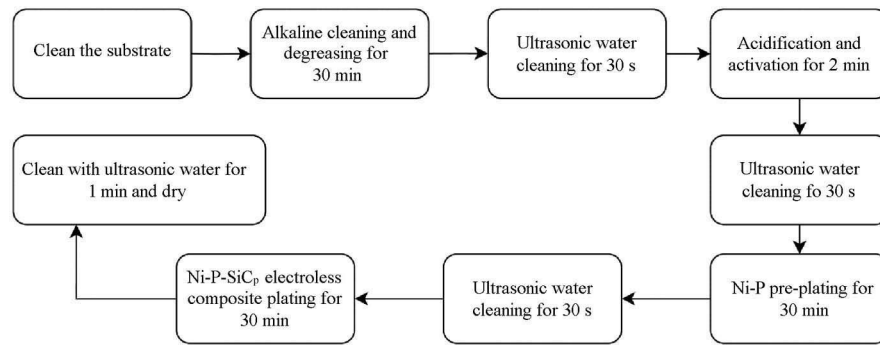Fig.2　Surface morphology after pre-plating Ni-P for 30 min

Fig.3   Process flow of electroless plating of Ni-P-SiC$_p$ composite coating
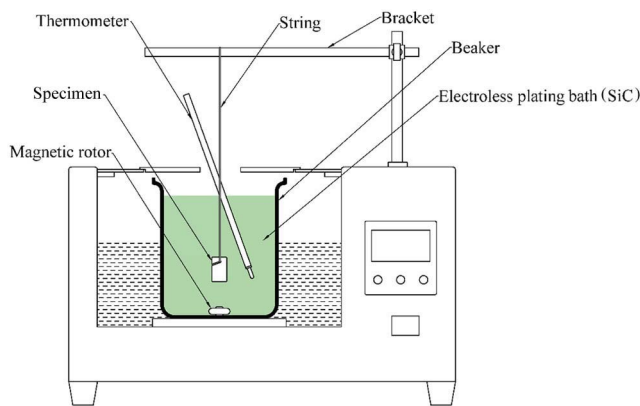

Fig.4   Schematic diagram of electroless plating experiment device

tube furnace under argon atmosphere. The specified heat treatment temperatures were 200, 350, 400, 450, 500, and 600 °C. The specimens were subjected to the designed temperature for 1 h, followed by gradual cooling to room temperature within the furnace.

HITACHIS-3400N scanning electron microscope (SEM) was employed to observe the surface morphology of the SiC$_p$ composite coatings at as-plated and heat-treated states. Oxford IE250 energy dispersive spectrometer (EDS) was used to analyze the composition of the composite coatings. For further analysis of morphology and composition of the worn surfaces, JXA-8230 electron probe coupled with EDS was applied. The phase structure of the composite coatings at as-plated and heat-treated states was analyzed using D/Max-2200 X-ray diffractometer (XRD) with Ni-filtered Cu Kα radiation source (λ =0.1541 nm). The scanning parameters were as follows: accelerating voltage of 40 kV, current intensity of 150 mA, scanning range of 10°−90°, scanning step of 0.04°, and scanning rate of 5°/min. HVS digital microscopic Vickers hardness tester was used to measure the microhardness of Ni-P-SiC$_p$ composite coatings. At least six points were measured for each specimen, and the average hardness value was used for analysis.

The industrial camera HW4K was used to observe the surface appearance of the worn specimen. Through calibration, the width of the wear scar could be obtained. Friction and wear tests were conducted on the as-plated and

heat-treated Ni-P-SiC$_p$ composite coatings as well as original substrate by the M-2000 wear testing machine. GCr15 material served as the counter grinding pair with hardness of 60.8 HRC. The specimen size was 10 mm×10 mm×7 mm, the load was 196 N, the counter grinding ring rotation speed was 200 r/min, the friction torque range was 0−5 N·m, and the sampling time was 0.5 s. A total of 1000 sampling points were taken during the wear process. The specimens were weighed before and after wear tests using the XEL200 electronic balance with measurement accuracy of 0.0001 g.

CHI660E electrochemical workstation was employed to measure the polarization curves of the as-plated and heat-treated Ni-P-SiC$_p$ composite coatings as well as original substrate in a 3.5wt% NaCl solution. The three-electrode system with reference electrode, working electrode, and counter electrode was used. The scanning rate was 0.001 mV/s, the tested specimen was sealed with epoxy resin, and the exposure area was only 1 cm^2.

2 Results and Discussion

2.1 Surface morphology and phase structure of Ni-P-SiC$_p$ composite coatings

Fig. 5 shows SEM surface morphologies of the Ni-P-SiC$_p$ composite coatings prepared under different SiC$_p$ concentrations. The surfaces exhibit cauliflower-like cellular structures and smooth dense surfaces without any apparent defects. Fig. 5a shows the surface of single Ni-P coating without SiC$_p$ addition, revealing large cell sizes and clear interfaces between cells. After SiC$_p$ addition, as shown in Fig.5b–5f, the cell sizes of the Ni-P-SiC$_p$ composite coatings are significantly refined, and the interfaces between cells become blurred. Simultaneously, SiC$_p$ is more distributed in the Ni-P coatings, and it is co-deposited with Ni and P on the substrate surface, which is consistent with the results in Ref.[31–33]. It is declared that the SiC$_p$ addition contributes to the refinement of cellular structures in the Ni-P coating. The negative charge on the surface of SiC$_p$ after infiltration treatment results in the adsorption of numerous Ni^{2+} ions onto the surface. During the solute migration, these ions are deposited on the substrate surface, serving as crystal nuclei, providing more nucleation points for metal plating growth, and ultimately refining the cellular structure of Ni-P plating. Additionally, as a hard
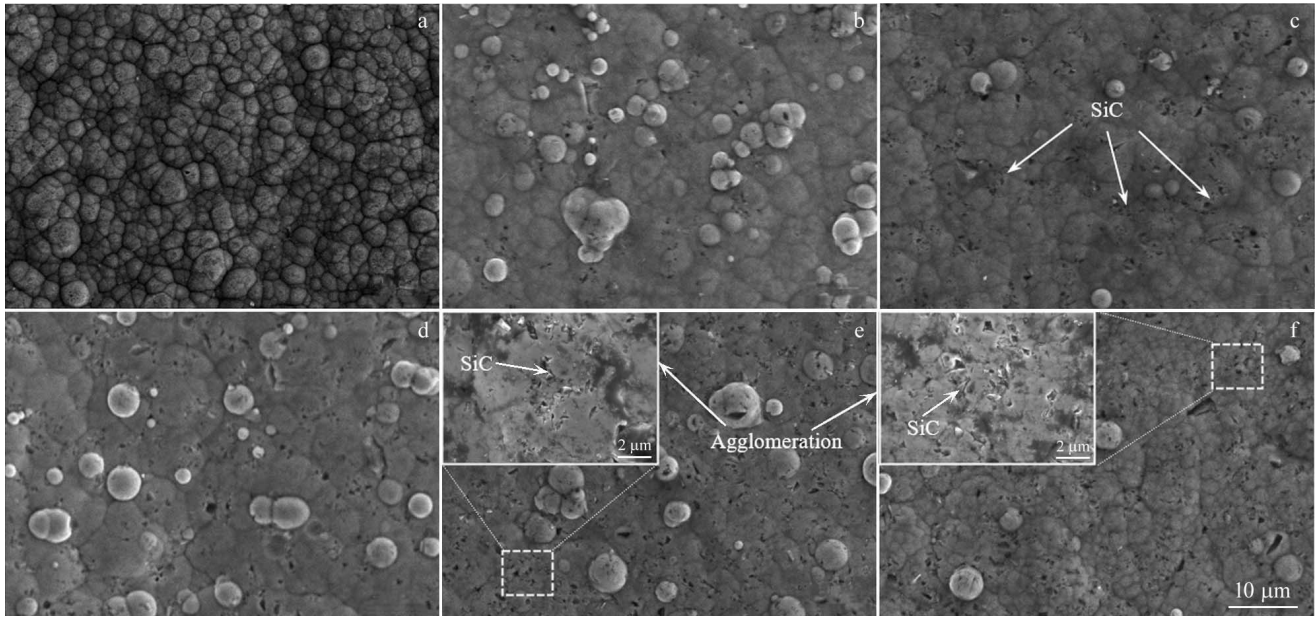
Fig.5　SEM surface morphologies of Ni-P-SiC$_P$ composite coatings prepared under different SiC$_P$ concentrations: (a) 0 g/L; (b) 1 g/L; (c) 3 g/L; (d) 5 g/L; (e) 7 g/L; (f) 9 g/L

second phase, SiC$_P$ is co-deposited with Ni and P on the substrate surface, playing a pinning role to imped the growth of Ni-P crystal nuclei and thereby refining the grains. Furthermore, Fig.5b–5f show that the density of co-deposited SiC$_P$ rises with the increase in SiC$_P$ concentration, leading to a reduction in the size of cells on the surface of Ni-P-SiC$_P$ composite coatings. Notably, when SiC$_P$ concentration is 7 and 9 g/L, agglomeration of SiC$_P$ on the coating surface is evident, as shown in Fig.5e and 5f.

Table 3 presents the contents of Ni, P, Si, and C elements on the surface of Ni-P-SiC$_P$ composite coatings prepared at various SiC$_P$ concentrations. The results reveal a notable increase in Si content within the coating as the SiC$_P$ concentration rises. However, this upward trend begins to slow down once the SiC$_P$ concentration exceeds 7 g/L. Conversely, the P content exhibits a significant decline trend with the increase in SiC$_P$ concentration. Simultaneously, a downward trend in Ni content can be observed. But compared with the variation trend of P content, the change in Ni content becomes relatively gentle when the SiC$_P$ concentration exceeds 3 g/L. The Ni:P ratio results of each composite coating reveal a general increase as the SiC$_P$ concentration

rises. This phenomenon suggests that during the co-deposition process of SiC$_P$ with Ni and P, SiC$_P$ can enhance the Ni deposition and inhibit the P deposition. This phenomenon can be attributed to the rise in Ni^{2+} ion adsorption on the SiC$_P$ surface, promoting Ni deposition. Furthermore, SEM morphology analysis of the Ni-P-SiC$_P$ composite coatings (Fig. 5) confirms that SiC$_P$ contributes to the nucleation of nickel grains during co-deposition, which consequently hinders the cellular growth and refines the cellular structure.

Fig. 6 illustrates XRD patterns of both substrate and Ni-P-SiC$_P$ composite coatings prepared under different SiC$_P$ concentrations. Distinct diffraction peaks at 45°, 65°, and 84° are evident in XRD patterns of both substrate and Ni-P-SiC$_P$ composite coatings. The Fe diffraction peak belongs to the substrate, whereas the Ni diffraction peak belongs to Ni-P-SiC$_P$ composite coating. Because Fe and Ni are transition metals with similar crystal structures, lattice constants, and crystal arrangements, their diffraction peak positions coincide, as

Table 3　Element contents of Ni-P-SiC$_P$ composite coatings prepared under different SiC$_P$ concentrations

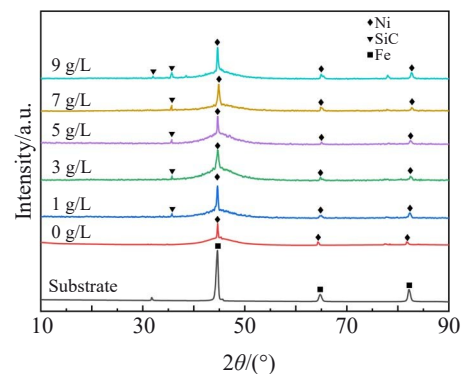| SiC$_P$ concentration/g·L^{-1}	0	1	3	5	7	9
C/wt%	-	23.85	31.86	30.53	30.30	30.70
Si/wt%	-	2.08	4.14	7.31	8.06	8.66
P/wt%	12.81	7.82	7.17	4.77	4.48	4.00
Ni/wt%	87.19	66.25	56.83	57.39	57.16	56.46
Ni:P ratio	6.8	8.47	7.93	12.03	12.75	14.12

Fig.6　XRD patterns of substrate and Ni-P-SiC$_P$ composite coatings prepared under different SiC$_P$ concentrations

shown in Fig. 6. In Ni-P-SiC$_P$ composite coatings, diffuse diffraction peaks appear around $2\theta=45°$, indicating the typical amorphous structural characteristics of Ni-P coatings[34–35]. Notably, with the increase in SiC$_P$ concentration, the width of diffraction peak becomes narrower, and the diffraction peak intensity of Ni phase shows a rising trend. This result suggests that the addition of SiC$_P$ facilitates the transformation of Ni-P coating from amorphous state to microcrystalline state. The composition analysis results in Table 3 align with this conclusion, confirming that SiC$_P$ has an inhibitory effect on P deposition. Furthermore, in Ni-P-SiC$_P$ composite coating, the diffraction peak of SiC ($2\theta=35°$) can be observed. With the increase in SiC$_P$ concentration, the intensity of SiC diffraction peak is also improved. It is important to note that due to the low SiC$_P$ concentration, the intensity of the detected SiC diffraction peak remains relatively low.

2.2 Microhardness and corrosion resistance of Ni-P-SiC$_P$ composite coatings

The microhardness results of the substrate and Ni-P-SiC$_P$ composite coatings prepared under different SiC$_P$ concentrations are shown in Fig.7. The microhardness of the 42CrMo substrate is approximately 3645.6 MPa. Notably, the microhardness of the Ni-P-SiC$_P$ composite coatings is significantly higher than that of the substrate. Moreover, the microhardness is firstly increased and then decreased with the increase in SiC$_P$ concentration. The peak microhardness of 7379.4 MPa is achieved when the SiC$_P$ concentration is 5 g/L. This result indicates the significant enhancement in coating microhardness resulting from the co-deposition of SiC$_P$ with Ni and P on the substrate surface. The collaborative effects of SiC$_P$ during co-deposition include the promotion of Ni nucleation, grain refinement, and facilitation of structural densification. The uniform distribution of SiC$_P$ on the Ni-P coating surface exerts dispersion strengthening effect, effectively impeding the plastic deformation under external forces[36] and thereby contributing to the microhardness improvement. Excessive SiC$_P$ concentrations (7 and 9 g/L) lead to aggregation. Although SiC$_P$ can refine the grains, the non-uniform distribution of SiC$_P$ impedes surface structure homogenization and densification, restricting the dispersion
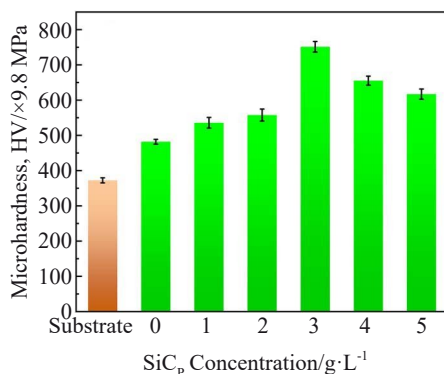
strengthening effect. Consequently, a decline in microhardness can be observed, but the microhardness remains higher than that of the substrate and the Ni-P coating without SiC$_P$ addition.

Fig. 8 shows the polarization curves of substrate and Ni-P-SiC$_P$ composite coatings prepared under different SiC$_P$ concentrations, and the corresponding calculated corrosion potential (E_{corr}) is presented in Table 4. Each anode potentiodynamic polarization curve exhibits an active-passive transition zone. Comparative analysis reveals that the corrosion potential of the Ni-P-SiC$_P$ composite coatings is significantly higher than that of the substrate, indicating excellent corrosion resistance. Notably, the corrosion resistance of Ni-P-SiC$_P$ composite coatings is significantly better than that of the substrate and Ni-P plating without SiC$_P$. It is concluded that the SiC$_P$ with excellent corrosion resistance can act as an inert physical barrier to prevent the corrosion of Ni-P coating by certain erosive electrolytes after co-deposition of SiC$_P$ with Ni and P on the substrate surface. Moreover, the corrosion potential of Ni-P-SiC$_P$ composite coatings is increased with the increase in SiC$_P$ concentration. But when the SiC$_P$ concentration exceeds 7 g/L, the corrosion potential begins to decrease. This decline is attributed to the SiC$_P$ agglomeration with excess SiC$_P$ addition, adversely affecting the uniformity and compactness of the coatings. Consequently, microcracks or microcavities may form on the coating surface, diminishing the corrosion resistance. Nevertheless, even at higher SiC$_P$ concentrations,
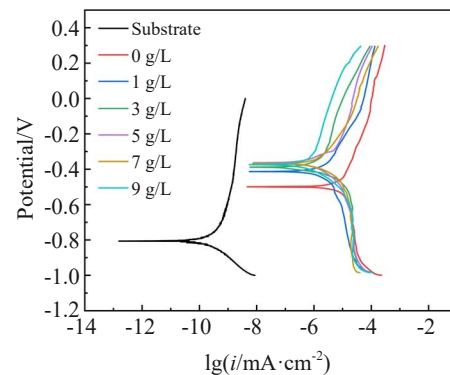
Fig.8   Polarization curves of substrate and Ni-P-SiC$_P$ composite coatings prepared under different SiC$_P$ concentrations

Table 4   Electrochemical corrosion potentials of substrate and Ni-P-SiC$_P$ composite coatings prepared under different SiC$_P$ concentrations

SiC$_P$ concentration/g·L^{-1}	E_{corr}/V
Substrate	−0.806
0	−0.449
1	−0.413
3	−0.388
5	−0.363
7	−0.368
9	−0.374

Fig.7   Microhardness of substrate and Ni-P-SiC$_P$ composite coatings prepared under different SiC$_P$ concentrations

the corrosion resistance is still better than that of Ni-P coating without SiC$_P$.

Based on the comprehensive comparative analysis of surface morphology, composition, phase structure, micro-hardness, and corrosion resistance of Ni-P-SiC$_P$ composite coatings prepared at various SiC$_P$ concentrations, it is evident that the overall performance of the composite coatings is optimal when the SiC$_P$ concentration is 5 g/L. To further enhance the coating performance, the Ni-P-SiC$_P$ composite coatings prepared at SiC$_P$ concentration of 5 g/L are heat-treated in argon protective atmosphere. This treatment aims to release residual hydrogen and internal stress within the coatings, expecting to achieve performance improvement.

2.3 Effect of heat treatment on Ni-P-SiC$_P$ composite coatings

2.3.1 Surface morphology of Ni-P-SiC$_P$ composite coatings after heat treatment

Fig. 9 shows the surface morphologies of Ni-P-SiC$_P$ composite coatings after heat treatment at various temperatures for 1 h, still exhibiting the characteristic cauliflower-like cellular structure[37]. Compared with the surface morphology of as-plated Ni-P-SiC$_P$ composite coating (Fig. 5d), after heat treatment at 200 °C, there is no obvious change in the size of surface cells. However, with the increase in heat treatment temperature, the size of the surface cells is initially increased and then decreased. Notably, after heat treatment at 500 °C, fine and dispersed white precipitates appear on the coating surface. Considering the chemical reaction deposition principle, substantial hydrogen is generated during the chemical deposition process, and some hydrogen may remain trapped within the Ni-P-SiC$_P$ composite coatings during co-deposition. After heat treatment at 200 °C, the primary effects of heat treatment include hydrogen release and stress relaxation, resulting in insignificant changes in the

surface morphology and cell size of the coatings[38–39].

When the heat treatment temperature rises, residual hydrogen atoms are precipitated, effectively alleviating internal stress, and the miniature cauliflower unit cells begin to coalesce with multiple small unit cells merging into larger unit cells. After heat treatment at 400 °C, the size of unit cells on the coating surface reach the maximum, resulting in a smooth and dense surface. After heat treatment at 450 °C, the cell size begins to decrease and continues to decrease with the further increase in heat treatment temperature. Fine and diffuse white precipitates on the surface can effectively impede the boundary expansion, slip, and dislocation of nickel grains, thereby refining the cell size and blurring the boundaries.

2.3.2 Phase structure and properties of Ni-P-SiC$_P$ composite coatings after heat treatment

Fig. 10 presents XRD patterns of Ni-P-SiC$_P$ composite coatings prepared under 5 g/L SiC$_P$ after heat treatment at different temperatures. Compared with the as-plated Ni-P-SiC$_P$ composite coating (Fig. 6), it can be seen that after heat treatment at 200 °C, the composite coating retains its typical amorphous structure. When the heat treatment temperature increases to 350 °C, the precipitation of the Ni$_3$P phase within the composite coating indicates the initiation of crystallization transformation. With the further increase in heat treatment temperature, structure relaxation occurs in the composite coating[40], accompanied by enhancement of P diffusion ability. Consequently, the precipitated Ni$_3$P phase continues to increase, leading to a gradual increase of the diffraction peak intensity of the Ni$_3$P phase, which agrees with the results in Ref. [41–43]. EDS analysis result of the white precipitate in Fig. 9e indicates that these fine dispersed white precipitates are the crystalline Ni$_3$P phase[44]. According to Fig. 10, the diffraction peak intensity of SiC$_P$ remains relatively stable within the temperature range of 200–450 °C, but it increases when the heat treatment temperature continues to rise. This
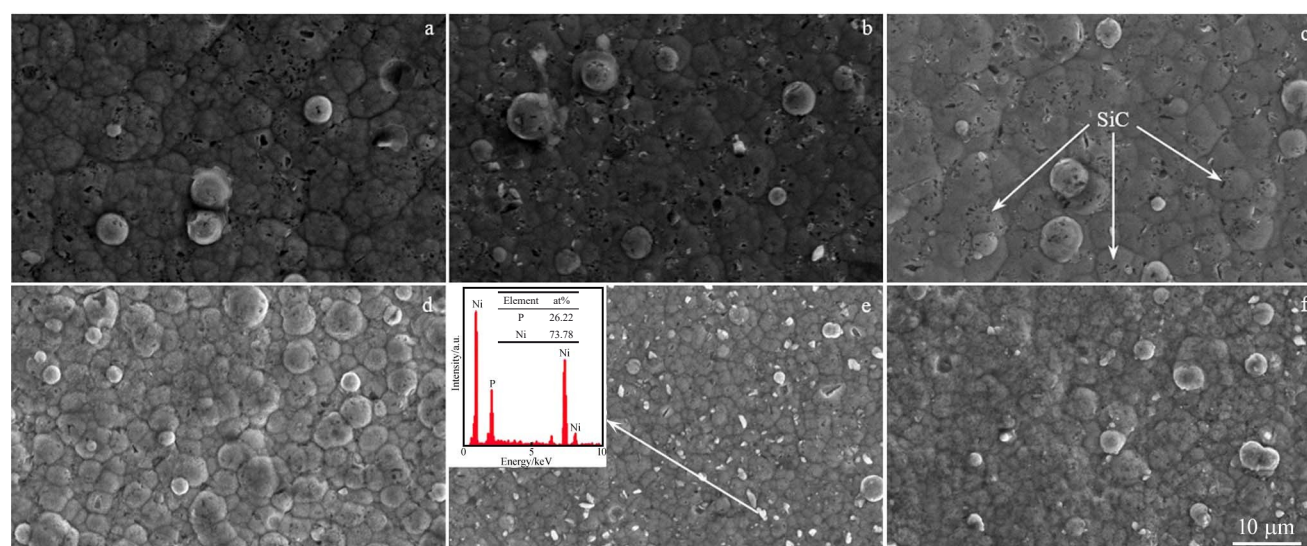

Fig.9   SEM morphologies of Ni-P-SiC$_P$ composite coatings prepared under 5 g/L SiC$_P$ after heat treatment at different temperatures: (a) 200 °C; (b) 350 °C; (c) 400 °C; (d) 450 °C; (e) 500 °C; (f) 600 °C
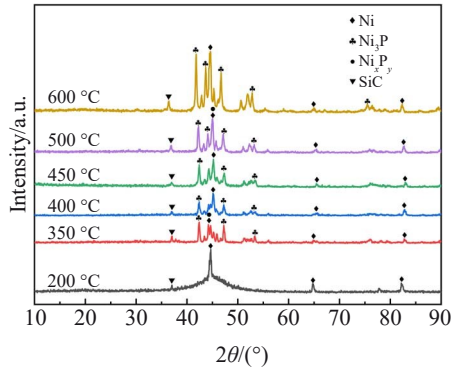
Fig.10   XRD patterns of Ni-P-SiC$_P$ composite coatings prepared under 5 g/L SiC$_P$ after heat treatment at different temperatures

phenomenon is attributed to the expansion of SiC$_P$ grains induced by the increasing temperature.

Fig.11 illustrates the microhardness of Ni-P-SiC$_P$ composite coatings with 5 g/L SiC$_P$ heat-treated at different temperatures. Compared with the microhardness of the as-plated Ni-P-SiC$_P$ composite coating with 5 g/L SiC$_P$ (7379 MPa), it can be seen that heat treatment can increase the microhardness of the Ni-P-SiC$_P$ composite coatings, and with the increase in heat treatment temperature, the microhardness of the Ni-P-SiC$_P$ composite coatings is firstly increased and then decreased, reaching the maximum value of 13 828 MPa (400 ° C). Combined with the above analysis of surface morphology and phase structure of Ni-P-SiC$_P$ composite coatings heat-treated at different temperatures, it becomes evident that the coating morphology and structure remain unchanged during heat treatment at 200 ° C. At this temperature, the composite coating mainly undergoes hydrogen release and stress relaxation, resulting in a slight increase in microhardness.

When the heat treatment temperature rises to 350 °C, the composite coating undergoes crystallization transformation, leading to the precipitation of the Ni$_3$P phase. At 400 °C, the crystallization transformation is completed, and the dispersed Ni$_3$P phase plays a pinning role in the Ni-P-SiC$_P$ composite coating, which refines the grains and enhances the compactness of the composite coating. The precipitated Ni$_3$P
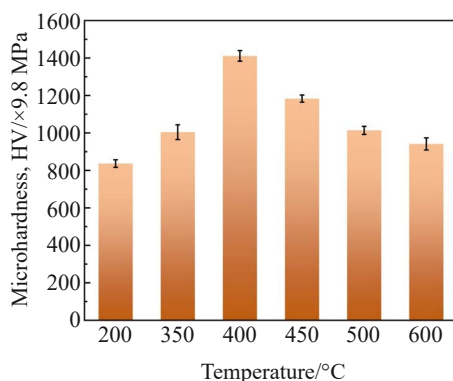
phase and the second phase SiC$_P$ dispersed in the composite coating play a synergistic role in strengthening precipitation and strengthening dispersion, therefore improving the plastic deformation slip resistance of the composite coating. The microhardness reaches the maximum value when the heat treatment temperature is 400 ° C. Once the heat treatment temperature surpasses 400 ° C, the precipitated Ni$_3$P phase begins to aggregate and grow. Besides, the higher the heat treatment temperature, the more intense the aggregation phenomenon, potentially causing coarse grain formation[45] and leading to a decline in the coating microhardness. Although the presence of SiC$_P$ in the composite coating inhibits the growth of Ni$_3$P phase, resulting in a more gradual decline in microhardness, the microhardness of Ni-P-SiC$_P$ composite coating after heat treatment is still significantly higher than that of the as-plated one.

Fig. 12 illustrates the polarization curves of the Ni-P-SiC$_P$ composite coatings heat-treated at different temperatures. Table 5 presents the corresponding calculated corrosion potential (E_{corr}) results. The corrosion potential of the composite coatings after heat treatment is higher than that of as-plated coating, indicating an enhancement in corrosion resistance of the Ni-P-SiC$_P$ composite coating due to heat treatment. With the increase in heat treatment temperature, the corrosion potential initially rises and then decreases. When the heat treatment temperature is 400 °C, the corrosion potential reaches its peak value, signifying the optimal corrosion resistance. This improvement in corrosion resistance is attributed to the release of residual hydrogen and stress during heat treatment, leading to the crystallization transformation in the Ni-P-SiC$_P$ composite coating. This process also results in the precipitation of a substantial amount of Ni$_3$P phase onto the Ni solid solution. The precipitated Ni$_3$P phase collaborates with the dispersed SiC$_P$ phase, acting as a pinning agent, thereby refining the coating structure, and enhancing the corrosion resistance.

At elevated heat treatment temperatures (exceeding 450 °C), the precipitated Ni$_3$P phase continues to increase and aggregate, but the presence of dispersed SiC$_P$ phase can hinder

Fig.11   Microhardness of Ni-P-SiC$_P$ composite coatings prepared under 5 g/L SiC$_P$ after heat treatment at different temperatures
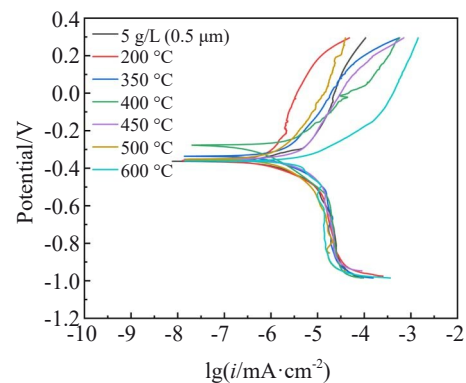

Fig.12   Polarization curves of Ni-P-SiC$_P$ composite coatings prepared under 5 g/L SiC$_P$ after heat treatment at different temperatures

Table 5   **Electrochemical corrosion potentials of Ni-P-SiC$_P$ composite coatings heat-treated at different temperatures**

Temperature/ °C	0	200	350	400	450	500	600
E_{corr}/V	−0.363	−0.359	−0.336	−0.277	−0.352	−0.352	−0.361

the growth and coarsening of Ni$_3$P phase. A mutual obstruction exists between two hard phases, resulting in more lattice distortion, twins, and other defects in the crystalline Ni-P-SiC$_P$ composite coating[46]. Consequently, the corrosion resistance diminishes, and after heat treatment at 600 °C, the corrosion potential of the Ni-P-SiC$_P$ composite coating becomes comparable to that of the as-plated one.

2.4 Wear resistance of Ni-P-SiC$_P$ composite coatings

Based on the abovementioned analysis, it is evident that the microhardness and corrosion resistance of the Ni-P-SiC$_P$ composite coating prepared under 5 g/L SiC$_P$ are superior, and they reach optimal state after heat treatment at 400 °C. Subsequently, friction and wear experiments were conducted on the substrate, Ni-P coating, and Ni-P-SiC$_P$ composite coating prepared under 5 g/L SiC$_P$ before and after heat treatment. Fig. 13 presents the appearances of the worn surfaces of the substrate, Ni-P coating, Ni-P-SiC$_P$ composite coating prepared under 5 g/L SiC$_P$ before heat treatment (as-plated coating), and Ni-P-SiC$_P$ composite coating prepared under 5 g/L SiC$_P$ after heat treatment at 400 °C (heat-treated coating). To comprehensively assess the wear resistance of these specimens, a comprehensive evaluation was conducted considering the wear amount and wear scar width after wear tests. Statistical data are summarized in Table 6.

Combining the analysis results of Fig. 13 and Table 6, it is inferred that the substrate has obvious furrow, the largest wear loss (0.0138 g), and the widest wear scars (width of 4.142

mm), indicating the worst wear resistance. The Ni-P coating has reduced wear loss (0.0101 g) and narrower wear scars (width of 3.120 mm), compared with the substrate, indicating a significant improvement in wear resistance. For the as-plated coating, the wear loss is 0.0016 g, and the width of the wear scar is 2.341 mm, showing good wear resistance. This improvement in wear resistance is attributed to the addition of SiC$_P$, which hinders the growth of Ni crystal nuclei, results in a more uniform and fine structure, and enhances the microhardness of Ni-P-SiC$_P$ composite coating. For the heat-treated coating, the wear loss is 0.0006 g, and the width of wear scar is 2.298 mm, indicating excellent wear resistance. The stress relaxation and structural changes during heat treatment improve the interface bonding force between the coating and substrate, and the crystallization transformation promotes the precipitation of Ni$_3$P phase, leading to significantly improved microhardness and excellent wear resistance. Compared with the Ni-P coating, the mass loss of as-plated coating (Ni-P-SiC$_P$ composite coating) is reduced by 84%. Khodaei et al[29] deposited Ni-P coatings with 1 g/L nano-SiC particles on carbon steel by electroless plating. The wear amount of the composite coatings after heat treatment was reduced by nearly 48%, compared with that of the Ni-P coating. Ram et al[47] showed that the mass loss of the heat-treated coating (Ni-P-SiC$_P$ composite coating after heat treatment) is reduced by 50%, compared with that of the Ni-P coating. It can be seen that the wear resistance of the Ni-P-SiC$_P$ composite coatings is better than that of coating with nano-SiC particles.

In Fig. 14a, there is obvious material accumulation on both sides of the wear scars on substrate, resulting in a rough surface with deep furrows, plough wrinkles, and severe adhesion. The worn surface displays serious abrasive and adhesive wear. Fig. 14e reveals that the worn surface is
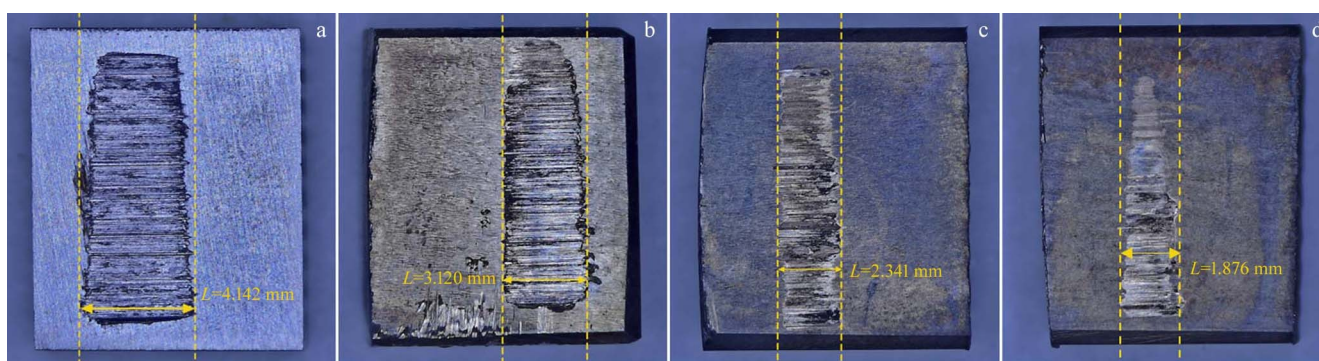

Fig.13   Appearances of worn surfaces and width of wear scars of substrate (a), Ni-P coating (b), as-plated coating (c), and heat-treated coating (d)

primarily composed of Fe element with a certain amount of O element, indicating oxidative wear due to frictional heat. Consequently, the wear mechanism of substrate primarily involves severe abrasive wear and adhesive wear, accompanied by some oxidative wear.

Fig. 14b shows the wear morphology of Ni-P coating, and the cellular structure can be observed on the worn surface.

Table 6   **Wear loss and scare width of substrate, Ni-P coating, as-plated coating, and heat-treated coating**

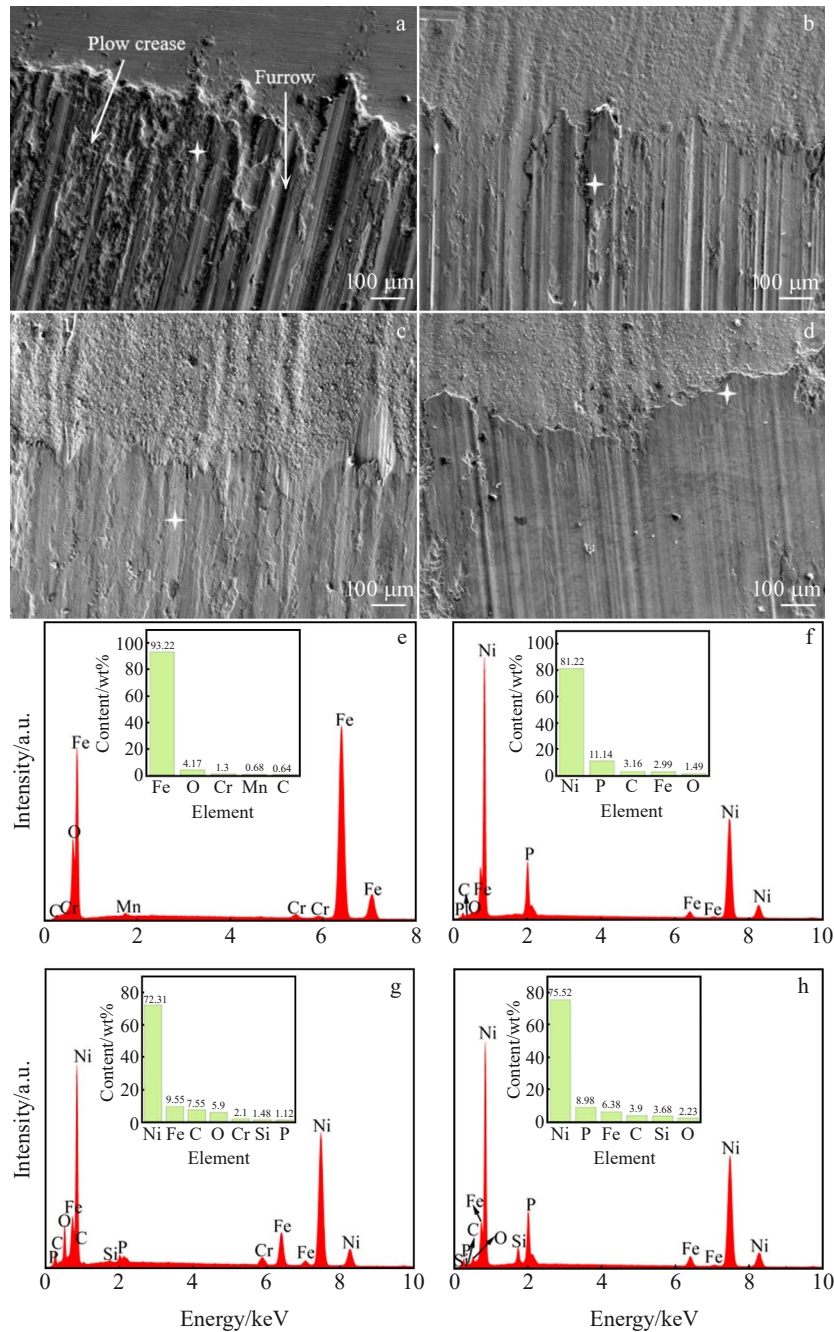| Specimen	Substrate	Ni-P coating	As-plated coating	Heat-treated coating
Wear loss/g	0.0138	0.0101	0.0016	0.0006
Scar width/mm	4.142	3.120	2.341	1.876

Fig.14   SEM wear morphologies (a–d) and EDS analysis results (e–h) of substrate (a, e), Ni-P coating (b, f), as-plated coating (c, g), and heat-treated coating (d, h)

Material accumulation around the wear scar is significantly reduced, compared with that of the substrate, resulting in a relatively flat worn surface with some shallow furrows. According to Fig. 14f, there is a certain amount of Fe and a small amount of O on the worn surface, suggesting that the material is transferred from the counter-grinding pair to the Ni-P coating. This phenomenon results in adhesive wear and slight oxidative wear under the influence of frictional heat. Consequently, the wear mechanism of the Ni-P coating primarily involves the abrasive wear, supplemented by adhesive wear and slight oxidation wear.

Fig. 14c shows the wear morphology of the as-plated

coating. A small amount of material accumulation can be observed on both sides of the wear scar, and the worn surface is smooth with a faint cellular structure. There are no obvious ploughing marks on the worn surface, which is mainly composed of rolling deformation layer formed by material transfer. Combined with the previous results, it can be seen that the addition of SiC_P enhances the uniformity, refinement, smoothness, and density of the Ni-P-SiC_P composite coating, and it significantly improves the microhardness. As shown in Fig.14g, there are Fe, Cr, and O elements on the worn surface, indicating that the wear mechanism of the as-plated coating primarily involves adhesive wear, accompanied by oxidative

wear to a small extent.

Fig. 14d shows the wear morphology of the heat-treated coating, and the worn surface is flat and smooth with only shallow grinding marks. After heat treatment, the composite coating undergoes the precipitation of hard Ni_3P phase, which promotes the SiC_P to enhance the plastic deformation resistance of the coating. Initial wear is attributed to the mutual friction within the actual contact area between the two friction pairs. As illustrated in Fig.14h, there is a small amount of Fe and O on the worn surface, indicating slight plastic deformation, material transfer due to the wear pair, and oxidation phenomenon due to frictional heat. Consequently, the wear mechanism of the $Ni-P-SiC_P$ composite coating prepared under 5 g/L SiC_P after heat treatment primarily involves micro-cutting abrasive wear, supplemented by slight adhesive wear and oxidative wear.

3 Conclusions

1) The surface of the electroless $Ni-P-SiC_P$ composite coatings exhibits a cauliflower-like cellular structure, and SiC_P are evenly distributed in the Ni-P coating. The $Ni-P-SiC_P$ composite coating displays typical amorphous structural characteristics. During the co-deposition of SiC_P with Ni and P, the SiC_P promotes Ni deposition and inhibits P deposition. The $Ni-P-SiC_P$ composite coating is gradually transformed into the microcrystalline structure with the increase in SiC_P concentration. The microhardness of $Ni-P-SiC_P$ composite coating prepared under 5 g/L SiC_P reaches the highest value of 7379 MPa, indicating optimal corrosion resistance.

2) The $Ni-P-SiC_P$ composite coating prepared under 5 g/L SiC_P undergoes heat treatment at different temperatures in an argon protective atmosphere. When the heat treatment temperature is 350 °C, crystallization transformation begins, and the Ni_3P dispersion strengthening phase is precipitated. The Ni_3P phase and the second hard phase SiC_P jointly enhance the microhardness and corrosion resistance. When the heat treatment temperature is 400 °C, the highest microhardness of 13 828 MPa and the corrosion potential of −0.277 V are achieved, indicating the optimal corrosion resistance.

3) The $Ni-P-SiC_P$ composite coating prepared under 5 g/L SiC_P after heat treatment at 400 °C exhibits the best wear resistance, and its wear mechanism is mainly micro-cutting abrasive wear, accompanied by slight adhesive wear and oxidative wear. The as-plated $Ni-P-SiC_P$ composite coating ranks second in wear resistance, and its wear mechanism is primarily adhesive wear, accompanied by certain oxidation wear.

References

1 Zamani S M, Hassanzadeh-Tabrizi S A, Sharifi H. *Engineering Failure Analysis*[J], 2016, 59: 605

2 Wen G, Guo X, Davies C. *Materials Technology*[J], 1999, 14(4): 210

3 Jothi S, Muraliraja R, Tamilarasan T *et al. Electroless Nickel Plating: Fundamental and Applications*[M]. Boston: CRC Press, 2019: 359

4 Ying L X, Liu Y, Liu G N *et al. Rare Metal Materials and Engineering*[J], 2015, 44(1): 28

5 Zheng Xiaohua, Liu Hui, Chen Li *et al. Rare Metal Materials and Engineering*[J], 2018, 47(S2): 171 (in Chinese)

6 Uppada S, Koona R, Chintada V B *et al. Silicon*[J], 2023, 15(2): 793

7 Luo H, Leitch M, Behnamian Y *et al. Surface and Coatings Technology*[J], 2015, 277: 99

8 Liu J, Zhao X, Yang Q *et al. Materials Letters*[J], 2023, 331: 133438

9 Du S M, Li Z, He Z T *et al. Tribology International*[J], 2018, 128: 197

10 Liang X H, Wu P G, Lan L X *et al. Materials*[J], 2023, 16(5): 1966

11 Ren A H, Kang M, Fu X Q. *Engineering Failure Analysis*[J], 2023, 143: 106934

12 Odiwo H, Bello K, Abdulwahab M *et al. Fundamental Journal of Sciences*[J], 2021, 5(1): 381

13 Zhou Wei, Xiao Peng, Li Yang *et al. Rare Metal Materials and Engineering*[J], 2017, 46(11): 3479 (in Chinese)

14 Liu G, Muolo M, Valenza F *et al. Ceramics International*[J], 2010, 36(4): 1177

15 Luo L M, Lu Z L, Tan X Y *et al. Powder Technology*[J], 2013, 249: 431

16 Chen J P, Gu L, He G. *Advances in Manufacturing*[J], 2020, 8: 279

17 Nirala A, Soren S, Kumar N *et al. Materials Today: Proceedings*[J], 2020, 21(3): 1610

18 Shukla M, Dhakad S, Agarwal P *et al. Materials Today: Proceedings*[J], 2018, 5(2): 5830

19 Sun R J, Cao Z W, Che Z G *et al. Surface and Coatings Technology*[J], 2022, 430: 127988

20 Chen Z, Yan Z J, Zhou H B *et al. Surface and Coatings Technology*[J], 2021, 409: 126876

21 Xu Y K, Wang G, Song Q *et al. Surface and Coatings Technology*[J], 2022, 437: 128349

22 Chintada V B, Gurugubelli T R, Koutavarapu R. *Materials Chemistry and Physics*[J], 2022, 291: 126682

23 Masallb H H, Kadhim A A. *BioGecko*[J], 2023, 12(2): 160

24 Liu G W, Luo W Q, Zhang X Z *et al. Rare Metals*[J], 2017, 42(2): 705

25 Gao P P, Gao M L, Wu A R *et al. Journal of Central South University*[J], 2020, 27(12): 3615

26 Farzaneh A, Mohammadi M, Ehteshamzadeh M *et al. Applied Surface Science*[J], 2013, 276: 697

27 Ahmadkhaniha D, Lattanzi L, Bonora F *et al. Coatings*[J], 2021, 11(2): 180

28 Ghavidel N, Allahkaram S R, Naderi R *et al. Surface and Coatings Technology*[J], 2020, 382: 125156

29 Khodaei M, Gholizadeh A M. *Materials Research Express*[J], 2021, 8(5): 055009

30 Liu Y S, Cheng L F, Zhang L T *et al. Materials Science and Engineering A*[J], 2008, 475(1–2): 217

31 Shu X, Wang Y, Liu C *et al. Materials Technology*[J], 2015, 30(S1): A41

32 Franco M, Sha W, Malinov S *et al. Surface and Coatings Technology*[J], 2013, 235: 755

33 Franco M, Sha W, Tan V *et al. Materials & Design*[J], 2015, 85: 248

34 Baskaran I, Narayanan T S, Stephen A. *Materials Chemistry and Physics*[J], 2006, 99(1): 117

35 Lin K L, Hwang J W. *Materials Chemistry and Physics*[J], 2002, 76(2): 204

36 Zhou Y, Xie F Q, Wu X Q *et al. Journal of Alloys and Compounds*[J], 2017, 699: 366

37 Mosayebi S, Rezaei M, Mahidashti Z. *Colloids and Surfaces A: Physicochemical and Engineering Aspects*[J], 2020, 94: 124654

38 Liu H, Yao H L, Thompson G E *et al. Surface Engineering*[J], 2015, 31(6): 412

39 Davoodi D, Emami A H, Vaghefi S M M *et al. International Journal of Pressure Vessels and Piping*[J], 2022, 200: 104823

40 Mayrhofer P H, Mitterer C, Hultman L *et al. Progress in Materials Science*[J], 2006, 51(8): 1032

41 Ma C Y, Wu F F, Ning Y M *et al. Ceramics International*[J], 2014, 40(7): 9279

42 Gao J J, Lui L, Wu Y T *et al. Surface and Coatings Technology*[J], 2006, 200(20–21): 5836

43 Malfatti C F, Ferreira J Z, Oliveira C T *et al. Materials and Corrosion*[J], 2012, 63(1): 36

44 Li Y, Bushby A J, Dunstan D J. *Proceedings of the Royal Society A: Mathematical, Physical and Engineering Sciences*[J], 2016, 472(2190): 20150890

45 Xiong J K, Wang D Y, Cai Y C *et al. Applied Physics A*[J], 2022, 128(4): 267

46 Shozib I A, Ahmad A, Abdul-Rani A M *et al. Corrosion Reviews*[J], 2022, 40(1): 1

47 Ram M, Sharma S, Ansari A *et al. AIP Conference Proceedings*[J], 2021, 2335: 080010

微纳SiC$_p$对化学镀Ni-P-SiC$_p$复合镀层组织和性能的影响

晁　爽[1]，曹晶晶[1,2]，李河宗[1,2]，范　磊[3]，杨军恒[1]，Harvey Christopher Martin[4]

(1. 河北工程大学 机械与装备工程学院，河北 邯郸 056038)
(2. 河北省智能工业装备技术重点实验室，河北 邯郸 056038)
(3. 中国矿业大学（北京） 机械与电气工程学院，北京 100083)
(4. 拉夫堡大学 航空与汽车工程系，英国 拉夫堡 LE11 3TU)

摘　要： 通过化学镀在42CrMo钢上沉积Ni-P-SiC$_p$复合镀层。分析了在不同热处理温度下加工的不同SiC$_p$浓度Ni-P-SiC$_p$复合镀层的表面形貌和相结构。研究了Ni-P-SiC$_p$复合镀层的显微硬度、耐腐蚀性和耐磨性。结果表明，Ni-P-SiC$_p$复合镀层呈现花椰菜状形貌。增加SiC$_p$浓度可以减小胞状物的尺寸。显微硬度和耐腐蚀性随着SiC$_p$浓度的增加而先增加后降低。当SiC$_p$浓度为5 g/L时，最大显微硬度和腐蚀电位分别为7379 MPa和-0.363 V。Ni-P-SiC$_p$复合镀层呈现非晶态结构，漫散衍射峰的宽度随着SiC$_p$浓度的增加而变窄。这表明SiC$_p$抑制了P的沉积，促进了微晶转变。在350 ℃下热处理后，Ni-P-SiC$_p$复合镀层结晶，导致Ni$_3$P相沉淀。在400 ℃下热处理1 h可使结构最大化。镀层中Ni$_3$P析出强化相和SiC$_p$弥散强化相的协同作用，促进了胞状组织的致密化，从而获得了最佳的显微硬度（13 828 MPa）、最佳的耐腐蚀性（-0.277 V）和优异的耐磨性。磨损机制以微切削磨料磨损为主，伴有轻微的粘着磨损和氧化磨损。

关键词： 42CrMo钢；Ni-P-SiC$_p$复合镀层；热处理；耐腐蚀性；磨损机理

作者简介：晁　爽，男，1997年生，硕士生，河北工程大学机械与装备工程学院，河北 邯郸 056038，E-mail：chaoshuangcs0127@163.com